Nanoscale zero-valent iron for aqueous lead removal

Yana Bagbi[1,3], Ankur Sarswat[2], Sachchidanand Tiwari[1], Dinesh Mohan[2], Arvind Pandey[3], Pratima R. Solanki[1*]

[1]*Special Centre for Nanosciences, Jawaharlal Nehru University, New Delhi, 110067, India*
[2]*School of Environmental Sciences, Jawaharlal Nehru University, New Delhi, 110067, India*
[3]*Department of Physics, North Eastern Regional Institute of Science and Technology, Nirjuli Arunachal Pradesh, 791109, India*

[*]Corresponding author, Tel: (+91)11-26704740; E-mail: pratimarsolanki@gmail.com; partima@mail.jnu.ac.in

Received: 08 February 2016, Revised: 29 July 2016 and Accepted: 03 August 2016

DOI: 10.5185/amp.2017/407
www.vbripress.com/amp

Abstract

Zero-valent iron nanoparticles (NZVI) were synthesized using chemical reduction method. These were applied for lead removal from water. The structural, morphological, compositional and optical studies were studied out using X-ray diffraction (XRD), transmission electron microscopy (TEM), dynamic light scattering, scanning electron microscopy (SEM) and Fourier transforms infrared spectroscopy (FTIR). The NZVI optical energy band gap as calculated by UV absorption spectrum was 1.7 eV. The zeta potential was obtained as -32.0 mV. The biocompatibility test of NZVI was performed using MTT assay on MDCK-2 as model cell lines. Lead adsorption on NZVI was examined at different pHs, equilibrium time, temperature, and NZVI/Pb^{2+} concentrations. Almost 100% Pb^{2+} removal was achieved at NZVI dose: 0.4 g/L; Pb^{2+} concentration: 50 mg/L; equilibrium time: 15 min; pH 5-6; and temperature: 25°C. Pb^{2+} sorption kinetic data were fitted to pseudo-first and second-order kinetic equations. Pseudo-second-order kinetic equation best fitted the data. These studies clearly demonstrate NZVI as an efficient nano-adsorbent for Pb^{2+} removal from water.

Keywords: Heavy metals, Pb^{2+} removal, zero-valent iron nanoparticles, lead adsorption, lead sorption studies.

Introduction

Heavy metal toxicity is one of the biggest environmental problems in this current industrial era. Wastewater discharge from chemical, metallurgical, battery manufacturing, leather tanning and mining industries contain heavy metal ions which directly or indirectly contaminate water bodies **[1, 2]**. Heavy metals are not only damaging the aquatic organisms but also getting enriched by precipitation and adsorption, harming human health through the food chain route **[1 - 3].** According to the World Health Organization (WHO), water pollution has led to the death of >3.5 million/year in which heavy metals contaminated drinking water is the primary leading cause **[3, 4]**.

Lead (Pb^{2+}) is one of the most shared and severe toxic metals commonly used in industries **[3]**. Lead is released in the environment by battery and paint industries and also from pipes used in water supply systems. The WHO and the Bureau of Indian Standards (BIS) have prescribed the maximum permissible limit of Pb^{2+} in drinking water at 0.01 mg/L **[5, 6]**. The United States Environmental Protection Agency (USEPA) allows a maximum permissible limit of lead in drinking water at 0.015 mg/L **[7]**. Accumulation of lead in humans can cause high blood pressure and anemia **[1-4, 8]**. Thus, Pb^{2+} removal from water bodies is required.

Chemical precipitation, reverse osmosis, electrochemical treatment technologies, ion exchange, membrane filtration, and adsorption were used for heavy metals remediation **[1, 9-10]**. Among them, adsorption is the most promising method due to its simplicity, and low cost **[11]**. Activated carbons **[12]**, clay minerals **[13]**, chelating materials **[14]** and chitosan/natural zeolites **[15]** were used to remediate heavy metal ions from water. Traditional sorbents were not very effective in lead removal and thus new and promising low cost adsorbents with high removal capacity and efficiency are required.

Recently, nanoscale zero-valent iron (NZVI) has been successfully used for heavy metals remediation from groundwater **[16, 17]**. NZVI is characterized by large surface area to volume ratio, less chemical consumption, faster removal kinetics, low cost and better injectability into aquifers **[16, 18]**. It was used to remove metallic and metalloid contaminants including Ni^{2+}, Co^{2+}, Cu^{2+}, CrO_4^{2-}, AsO_4^{3-} and AsO_3^{3-} from soil and water **[18-24]**. However, limited attempts have been made to explore NZVI for Pb^{2+} removal **[17, 21-28]**. Polyacrylic acid (PAA) stabilized NZVI exhibited 90% lead removal within 15 min **[26]**. A zeolite (Z) and NZVI composite remediated

96% lead within 140 min **[27]**. However, kaolinite supported NZVI removed 96% of Pb^{2+} in 30 min **[28]**. Disposal of metal ions loaded nano-adsorbent is also important. Only few studies on detoxification and regeneration of nanoadsorbents are available **[3, 4]**.

Herein, zero valent iron nanoparticles (NZVI) were synthesized by chemical reduction method using $FeCl_3 \cdot 6H_2O$ and sodium borohydride ($NaBH_4$). NZVI was characterized for its physical and optical properties and used for lead remediation from water. Lead adsorption on NZVI was studied at different pHs, time intervals, temperature, and NZVI/Pb^{2+} concentrations. Biocompatibility test is necessary before nano-adsorbent is applied to water treatment. Thus, biocompatibility test NZVI using MTT assay on MDCK-2 as model cell lines was investigated. A possible mechanism for Pb^{2+} adsorption on NZVI was also discussed.

Experimental

Materials

Ferric chloride [$FeCl_3 \cdot 6H_2O$] (99%), sodium borohydride ($NaBH_4$) (99%), lead nitrate [Pb $(NO_3)_2$] (98%) were purchased from Sigma-Aldrich, USA. Hydrochloric acid (N/10) and sodium hydroxide (98%) were purchased from Merck, India. Dulbecco's modified Eagle medium (DMEM) high glucose, fetal bovine serum (FBS), antibiotic-antimycotic solution, Trypsin-EDTA solution 1X, Dimethyle sulphoxide (DMSO), Dulbecco's phosphate buffered saline 1X (DPBS) and 3-(4,5-dimethyle-2-thiazolyl)-2,5-diphenyl-2H-tetrazolium bromide (MTT) were procured from HiMedia Laboratories Pvt. Ltd India. A 5mg mL^{-1} MTT solution was prepared in DPBS with the help of shaker. Lead stock solution (1000 mg/L) was prepared by dissolving 1g of Pb $(NO_3)_2$ salts in 1000 mL deionized water.

Synthesis of NZVI NPs

NZVI was prepared using the $NaBH_4$ reduction method reported elsewhere **[29]**. Briefly, 14.2 g of $FeCl_3.6H_2O$ was dissolved in 50 mL ethanol and stirred for 4 h. Reducing agent was prepared by dissolving 7.2 g of sodium borohydride in 100 mL of deionized water and added dropwise (1drop/2 sec.) to aqueous Fe^{3+}. The suspension was vacuum filtered. The residue was washed thrice with 25 mL ethanol each time. The NZVI powder thus obtained was oven dried (50 ˚C overnight) (eqn. 1). **Scheme 1** shows the systematic representation of NZVI synthesis.

$$4Fe^{3+}_{(aq)} + 3BH_4 + 9H_2O \rightarrow 4Fe^{0}_{(s)} + 3H_2BO_3 + 12H^{+} + 6H_{2(g)} \quad (1)$$

Biocompatibility test

The effect of NZVI on cell line survival (MDCK-2) was studied using MTT assay. About 2×10^3 cells/well with 1% (FBS) DMEM were plated in 96-well tissue culture plate and incubated at 37ºC under 5% CO_2 atmosphere. After 24 h the cell medium was replaced by NZVI containing (different concentration) 1% DMEM medium and cells were incubated at 37 °C under 5% CO_2 atmosphere for 24h. The NZVI was dispersed in DMEM medium by continuous sonication. This suspension was kept at room temperature for 1 h to allow the non-dispersed NZVI to settle down. Prior to the addition of dispersed NZVI to the growth medium, the NZVI was again dispersed by sonication using a sonicator bath at room temperature (10 min at 40 W). The dispersed nanoparticles are added to the cell growth medium at a final concentration of 5, 10, 20, 30, 40, 50 µg/mL.

After the incubation period, 20 µL of MTT (5mg mL^{-1} in DPBS) were added to each well. The cells were kept in dark for 3 h in a CO_2 incubator at 37 °C to allow the reduction of MTT dye to formazan crystal by living cells. Cells in each well were solubilized in 200 µL of DMSO and absorbance was recorded at 490 nm with the help of ELISA plate reader. The percentage proliferation change was calculated for control and exposed to NZVI. All experiments were carried out in triplicate.

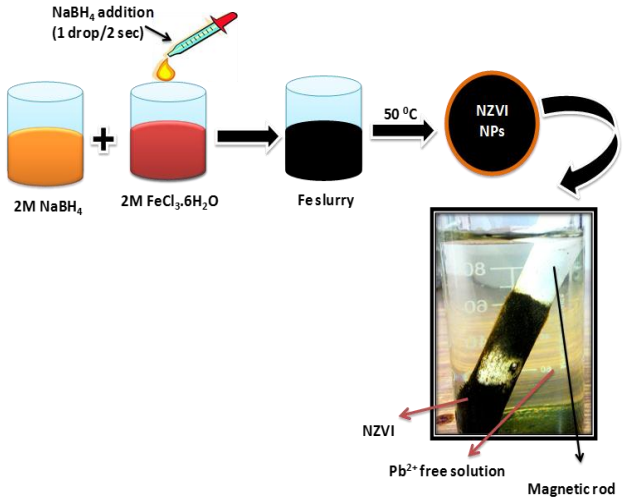

Scheme 1. Schematic diagram for NZVI synthesis.

Lead removal using NZVI

These studies were carried out in batch mode. An adsorbent dose of 0.4 g/L was used. Lead adsorption on NZVI was examined at different pH (2 to7), equilibrium time (2-30 min.), temperature (5-45 °C), and NZVI/Pb^{2+} concentrations. The pH was adjusted using 0.1 M HCl or 0.1M NaOH solutions. In all the kinetic studies, samples were shaken vigorously at 200 rpm for 60 minutes. After a pre-decided interval of time, suspensions were filtered using Whatman filter paper No.42 and lead concentration in filtrate was determined using atomic absorption spectrophotometer. The Pb^{2+} adsorption was calculated using equation 2.

$$q_e = \frac{(C_0 - C_e)V}{W} \quad (2)$$

where, C_0 and C_e are the initial and equilibrium lead concentrations (mg/L), V is the volume (L), and W is the weight (g) of NZVI.

Kinetic studies were carried out at different pHs, adsorbate/adsorbent concentrations and temperatures. Lead kinetic data were fitted to pseudo-first and pseudo-second order rate equations **[30, 31]**.

Pseudo-first-order kinetic model

The linear and nonlinear pseudo-first-order rate equations are given by Lagergren **[30]**.

$$\log(q_e - q_t) = \log(q_e) - \frac{k_1}{2.303}t \quad \text{(Linear form)} \qquad (3)$$

$$q_t = q_e(1 - e^{-k_1 t}) \quad \text{(Nonlinear form)} \qquad (4)$$

where, k_1, (min^{-1}) is the pseudo-first-order rate constant, q_e the amount of lead adsorbed at equilibrium, and q_t is the amount of lead adsorbed at time 't'.

Pseudo-second-order kinetic model

A pseudo-second-order rate equation is given by Ho **[31]** (eqn. 5).

$$\frac{t}{q_t} = \frac{1}{k_2 q_e^{\,2}} + \frac{t}{q_t} \qquad (5)$$

where, k_2 (mol L^{-1} min^{-1}) is the pseudo-second-order adsorption rate constant q_e the amount of lead adsorbed at equilibrium, and q_t is the amount of lead adsorbed at time 't'. The product $k_2 q_e^{\,2}$ represents the initial sorption rate [Rate = $k_2 q_e^{\,2}$].

Characterization of NZVI

XRD spectrum of NZVI was recorded using X-ray diffractometer (model Rigaku D/Max 2200), Cu Kα radiation (λ =1.5406 Å; 2θ= 10˚ to 80˚; step size = 2˚/min). HT-TEM micrographs were obtained using transmission electron microscope (HRTEM) model JEOL JEM-2200 FS (Japan). Samples were prepared on amorphous carbon-coated copper grids and then dried at room temperature. Surface morphology of NZVI were obtained using scanning electron microscope (SEM) model JEOL JSM-6480 LV. Energy dispersive X-ray analyzer (model Zeiss, EVO40) equipped with SEM was used for elemental analysis. The optical study of NZVI was carried out using UV-VIS spectrophotometer (model Systronis-117) in the wavelength range of 200 to 600 nm. Functional groups were identified using FTIR spectrometer (model Varian 600 UMA)

Dynamic light scattering (DLS) measurements were performed at a scattering angle (θ) of 90^0 and a laser wavelength of He/Ne laser of λ=632.8 nm on RINA Netzwerk RNA- technologies. The instrument was used in the polarized mode to determine the hydrodynamic size of NZVI. The diffusion coefficient is related to corresponding effective hydrodynamic radius through Stoke−Einstein relation:

$$R_h = \frac{k_B T}{6\pi\eta D} \qquad (6)$$

where, the solvent viscosity is η, k_B is the Boltzmann constant, and T is the absolute temperature.

The zeta-potential measurements were performed on an electrophoresis instrument (model ZC-2000, Microtec, Japan). In the case of the interacting solutions, if one uses the zeta potential (Z) as an approximation of the surface potential φ of a uniformly charged sphere, the theory gives

$$Z \approx \varphi = 4\pi \left(\sigma/\varepsilon\kappa\right) \qquad (7)$$

where, σ is the surface charge density of the particle, and ε and κ are the dielectric constant and Debye-Huckel parameter of the solution, respectively. The relationship between the mobility (μ) and the zeta potential is $Z=4\pi(\mu\eta/\varepsilon)$. Next, μ can be written as $\mu=\sigma/\eta\kappa$, where η is the viscosity of the solution.

Initial and equilibrium lead concentrations in the samples were measured using atomic absorption spectrometer (model AAnalyst 400, Perkin Elmer) at 283.3 nm wavelength.

Results and discussion

Structural and morphological studies

Fig. 1(a) shows the XRD pattern of stabilized NZVI under ambient conditions recorded over a 2θ range of 10˚ to 80˚ to obtained size, phases and oxidation state. The dominant peak appeared at ~44.8° corresponds to the plane (110) (JCPDS 00-006-0696) **[29]**. No additional peak was appearing relating to any impurity. These results revealed that NZVI is polycrystalline in nature with the body centered configuration. The particle size of synthesized NZVI obtained from Scherer's equation

$$D = \frac{0.9\lambda}{\beta\cos\theta} \qquad (8)$$

where, D is the particle size in Å, λ the wavelength of Cu Kα radiation, i.e., 1.54 Å, β is the full width at half maximum (FWHM), and θ is the angle obtained from 2θ corresponding to maximum peak intensity. The mean crystalline dimension of the NZVI was found to be 11.6 nm. **Fig. 1(b)** shows the surface morphology of synthesized NZVI observed by SEM. This clearly demonstrates the evenly distributed globular structure of NZVI and formation of a porous surface. These globular structures may thus responsible in an increase in available surface area required for Pb^{2+} adsorption. However, HR-TEM measurement shows a spherical shape of NZVI. Chain-like aggregates formed due to magnetic and *van der Waals* attraction between adjacent particulates [**Fig. 2(a&b)**]. The size of NZVI varies from 50 to 90 nm [**Fig. 2(a)** inset]. Similar results were reported in earlier studies **[25, 28]**. The corresponding atomic-scale image [**Fig. 2(b)**] exhibits the well-organized lattice planes with an interfacing spacing of 0.453 nm. The hydrodynamics size of NZVI was 110 nm as calculated according to Stoke−Einstein relation (Eq. 6) (figure omitted for brevity). TEM and DLS data appear in good agreement.

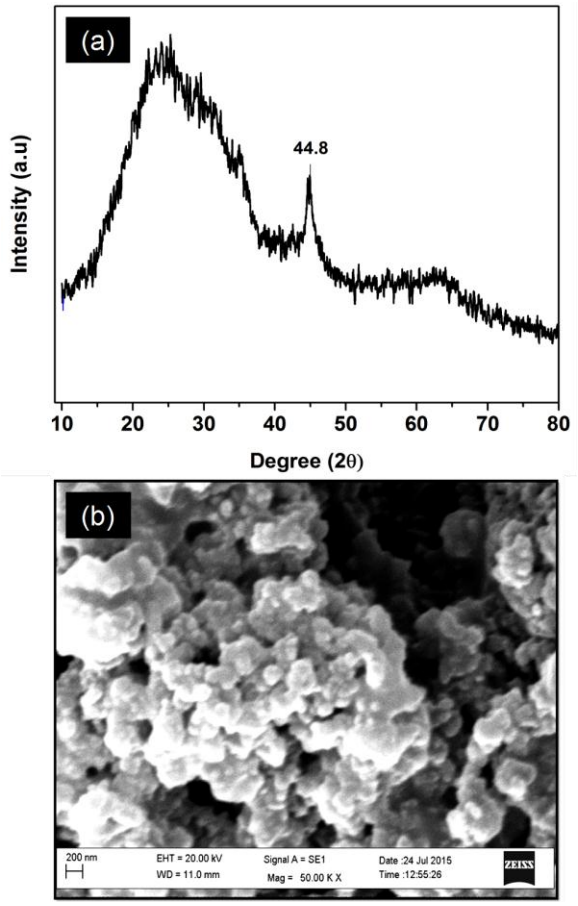

Fig. 1. (a) X-ray diffraction pattern of NZVI and (b) SEM micrographs of NZVI at 50 KX magnifications.

UV-vis spectrophotometer obtained the opticalabsorption spectrum and band gap energy of NZVI (figure omitted for brevity). Band gap was calculated using equation 9 given for a semiconductor.

$$\alpha = \frac{(Ahv - Eg)^{\frac{1}{2}}}{hv} \quad (9)$$

where, A is a constant and E_g is the energy band gap. When αhv = 0, Eg = hv. The band gap was calculated from the plot between $(\alpha hv)^2$ and hv by using the direct equation of Tauc plots. The absorption peaks obtained at 365 and 248 nm are assigned to a characteristic peak of monodispersed iron nanoparticles in zero valent states **[32].** The energy band gap of 1.7 eV was obtained for NZVI. This value is slightly higher to bulk iron i.e. E_g=1.5eV **[33, 34].** These results further confirmed the formation of nanosized NZVI particles.

The zeta potential of NZVI measurement has given the highly negative surface charge value of -32.0 mV (figure omitted for brevity).

Biocompatibility test

Fig. 3(i) shows the relative percentage proliferation/ survival of Madin-Darby canine kidney-2 (MDCK-2) cells in a different concentration of 5, 10, 20, 30, 40, 50 µg/mL of NZVI. NZVI shows a negative impact on the proliferation of MDCK-2 cells. The relative % proliferation of cells was calculated on the growth of control cells that was not exposed to NZVI. NZVI does not show any adverse effect on cell viability, thereby, indicating good biocompatibility.

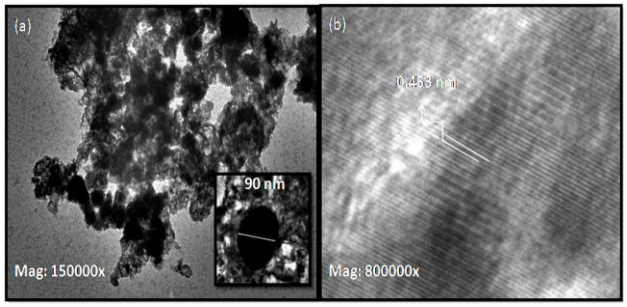

Fig. 2. TEM images of NZVI (a) at 150 KX and (b) at 800 KX magnifications. Inset (a) shows single NZVI.

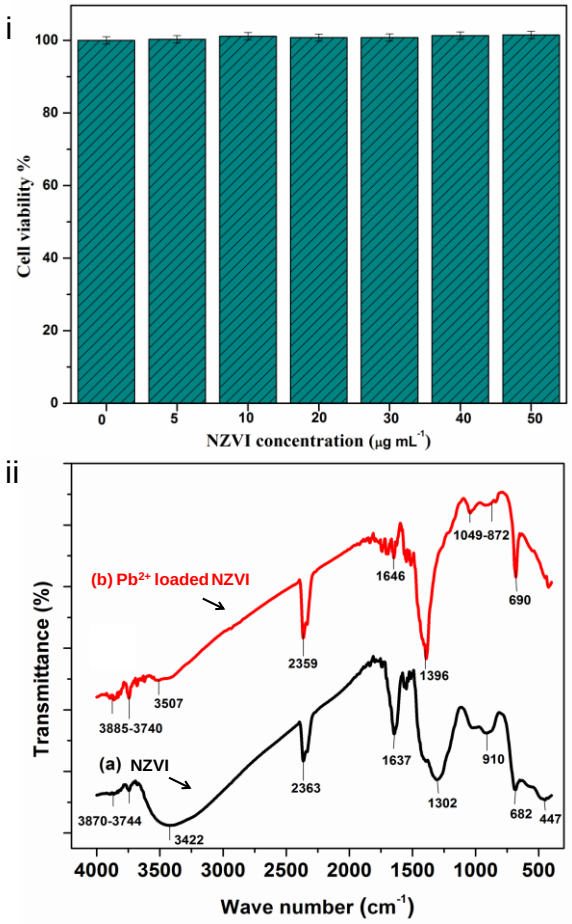

Fig. 3. (i) Cell viability (%) of MTT assay at different concentrations of NZVI and (ii) FTIR spectra of (a) NZVI and (b) Pb^{2+} loaded NZVI.

Structural interaction studies

Fig. 3(ii) shows the FTIR spectra of NZVI [curve (a)] and NZVI bind with Pb^{2+} after reaction [curve (b)] were obtained in the range of 400–4000 cm^{-1}. Furthermore, new absorption peaks observed at 447 and 682 cm^{-1} correspond to Fe-O stretching vibration. The band

appeared at 3422 and 1637 cm^{-1} [curve (a)] ascribe to O-H stretching and bending vibration band of water moiety adsorbed on NZVI surface. This suggests the formation of ferric oxyhydroxide (FeOOH) layer on NZVI **[27]**. The peaks at 1302 and 1100 cm^{-1} were shifted after Pb^{2+} adsorption, thereby, indicating the loss of water molecules **[26]**. The change in IR intensity between 1200 and 900 cm^{-1} suggested Pb^{2+} adsorption occurred in the form Fe-O-Pb with bending modes at 740 and 689 cm^{-1} **[36]**. IR peak intensity decreases at 1000 cm^{-1} [curve (b)], thereby, suggesting the breaking of hydrogen bond due to lead adsorption **[26]**.

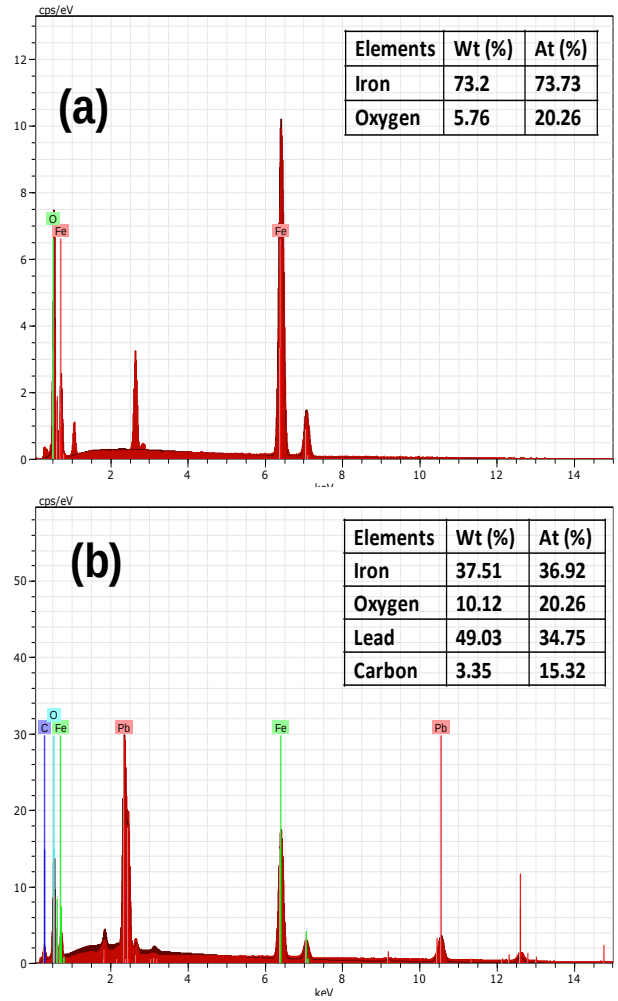

Fig. 4. (a) EDX spectra of NZVI and (b) NZVI loaded with Pb^{2+}. Inset table shows quantitative elemental analyses of NZVI.

Fig. 4 (a&b) shows the element analysis of NZVI. About 73% iron was measured. No impurities were observed in the EDX data. Table inserted in the image (b), represents the atomic percentage of elements. These results clearly show the purity of NZVI. Further confirmation of Pb^{2+} removal is shown in **Fig. 4 (a&b)**. Element analysis of lead loaded NZVI revealed the presence of Pb^{2+} (49.03%), and iron (37.51%). Trace amount of carbon (3.35%) was also recorded. This may be due to NZVI mounting by carbon tab as shown in Table inserted in the image (c).

Sorption studies

Effect of initial pH

pH plays an important role in affecting the solution chemistry. Speciation of lead changes with pH. Pb^{2+} exists in the pH range of 2.0 to 7.0. Lead ions start precipitating at a pH >7.0 **[35]**. Therefore, sorption studies were conducted in the pH range of 2.0 to 7.0 [Pb^{2+} conc. = 50 mg/L; equilibrium time= 30 min; agitation speed= 200 rpm]. Effect of pH on Pb^{2+} adsorption is shown in **Fig. 5(a)**.

Pb^{2+} adsorption is less between pH 2.0 to 3.0. Adsorption starts increasing after pH 4.0. At low pH (pH <4.0), Pb^{2+}affinity for available adsorption sites is weak. This may be due to the availability of H_3O^+ ions. With rise in pH, the solution becomes less acidic and conditions are favorable for Pb^{2+} adsorption. Also, deprotonation results into more negatively charged sites on NZVI. These deprotonates sites bind Pb^{2+} through electrostatic attraction **[26-28]**.

Effect of equilibrium time

Effect of contact time on Pb^{2+} removal was investigated at different time intervals (2 to 30 minutes; NZVI dose= 0.4 g/L; pH= 5.0; agitation speed= 200 rpm). The adsorption process is very fast and equilibrium was reached within 15 min [**Fig. 5(b)**]. Pb^{2+} removal after 15 minutes was not significant **[27-28]**.

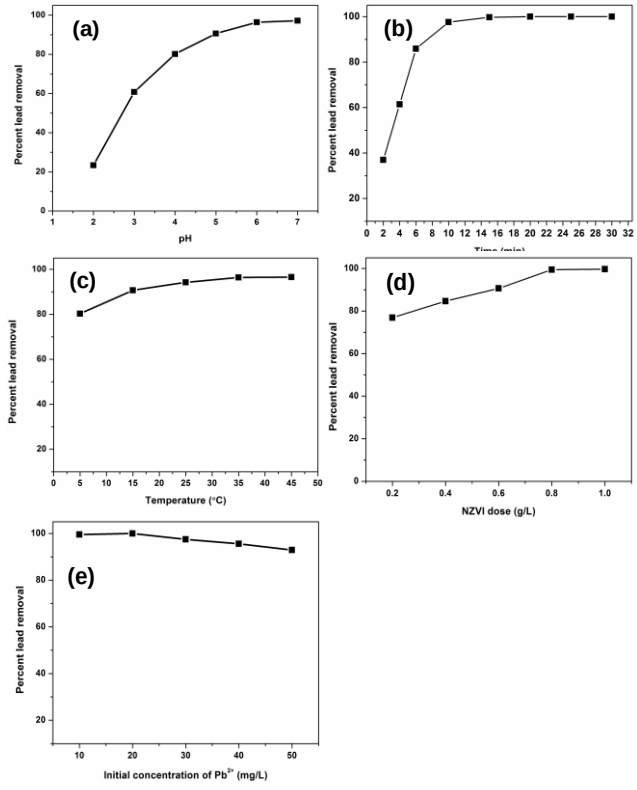

Fig. 5. Factor effecting the removal of Pb^{2+} using NZVI;(a) Effect of pH (2-7); (b) Effect of reaction time (2-30 min); (c) Effect of reaction temperature (5-45 °C); (d) Effect of NZVI dosage (0.2-1.0 g/L); (e) Effect of initial Pb^{2+} concentration (10-50 mg/L).

Effect of temperature

Dynamic studies were also carried at 5, 15, 25, 35 and 45 °C [**Fig. 5(c)**]. Pb^{2+} removal increased with increase in temperature, thereby, indicating the adsorption process to be endothermic in nature. There may be a possibility of pore broadening and expansion with rise in temperature **[35]**. Furthermore, there is also a possibility of internal bonds breaking at edges at high temperature **[26, 36]** resulting into more lead adsorption.

Effect of NZVI dose

Dose optimization for a sorption process is an essential step. Pb^{2+} removal was investigated at 0.2, 0.4, 0.6, 0.8 and 1.0 NZVI dosage (pH= 5.0; Pb^{2+} concentration = 50 mg/L; equilibrium time= 30 minutes; agitation speed = 200 rpm) [**Fig. 5(d)**]. Pb^{2+} was increased from 74 to ~100% when NZVI dose was increased from 0.2 to 1.0 g/L. This may be due to the availability of more adsorption sites at higher dose 0.8 g/L. No further Pb^{2+} uptake was observed at higher dosage.

Effect of initial Pb^{2+} concentration

Dynamic studies were also conducted at 10, 20, 30, 40 and 50 mg/L Pb^{2+} concentrations (pH= 5.0, NZVI dose = 0.4 g/L, agitation speed= 200 rpm) for 30 minutes [**Fig. 5(e)**]. Pb^{2+} removal was moderately affected with increase or decrease in lead concentrations. Almost complete Pb^{2+} removal (>95%) was obtained at various concentrations.

Kinetic modeling

Pseudo-first-order and second-order kinetic models were used to fit data. **Fig. 6** shows Pb^{2+} removal kinetic using pseudo-second-order rate equation. Second order model better fitted the data (R^2= 0.9776), thereby, indicating that Pb^{2+} sorption on NZVI was controlled by chemisorption **[27, 37]**. The obtained kinetic parameters, i.e., regression coefficients (R^2) and rate constants (k) are illustrated in **Table 1**.

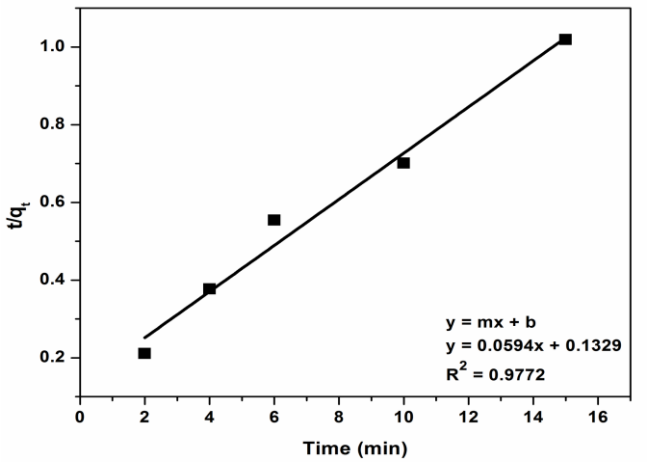

Fig. 6. Pseudo-second-order kinetic plot for Pb^{2+} adsorption by NZVI (NZVI dose= 0.4 g/L; Pb^{2+} concentration= 50 mg/L; pH= 5.0; temperature= 25 ºC).

Table 1. Kinetic parameters for lead removal.

Kinetic parameters	Pseudo-first-order	Pseudo-second-order
K	0.155	0.059
R^2	0.950	0.977

Table 2. Comparative evaluation of kinetic parameters obtained for NZVI versus other nano-adsorbents.

Nanomaterials	Dose (g/L)	Pb^{2+} conc. (mg/L)	R^2	Equilibrium time (min)	Ref.
Amine-functionalized Fe_3O_4 (AF-Fe_3O_4)	0.01	5	0.9983	120	38
Functionalized magnetite (RB-MMNPs)	0.02	50	0.9997	30	39
NZVI supported on sineguelas	0.15	10	0.9999	60	25
(S-NaOH-NZVI)			1.0		
			1.0		
Graphene composite NZVI (G-NZVI)	0.2	250	0.999	240	40
			0.999		
Polyacrylicacid-Stabilized NZVI (PAA-ZVIN)	2	10	0.8872	15	26
Fe_3O_4/SiO_2-NH_2	0.05	10	0.999	120	41
			0.989		
			0.994		
	1	25	0.999		35
	1	50	0.999		
Magnetite	1	100	0.991	1440	
Nanoparticles	0.5	-	0.996		
	1.0	-	0.999		
	1.5	-	0.999		
NZVI	0.4	50	0.977	15	Present work

Conclusion

NZVI NPs were synthesized following reduction method. NZVI was characterized using XRD, SEM, TEM, DLS, UV-Vis, Zeta potential and FT-IR studies. Furthermore, cytotoxicity of NZVI was investigated through MTT assay using MDCK-2 as model cell lines. Pb^{2+} was successfully remediated using NZVI in batch mode under various experimental parameters [solution pH, equilibrium time, temperature, NZVI/Pb^{2+}concentration]. Almost 100% Pb^{2+} removal was achieved at NZVI dose: 0.4 g/L; Pb^{2+} concentration: 50 mg/L; equilibrium time: 15 min; pH 5-6; and temperature 25 °C. Pb^{2+} sorption kinetic data were fitted to pseudo-first and second-order kinetic equations. Pseudo-second-order kinetic equation best fitted the data, thereby, indicating that chemisorption was the rate determining step for Pb^{2+} removal. The data is better or comparable to other nanoadsorbents used for lead removal (**Table 2**). These studies clearly demonstrate NZVI as an efficient biocompatible nano-adsorbent for Pb^{2+} removal.

Acknowledgements

We acknowledge Advanced Instrumentation Research Facility Jawaharlal Nehru University (JNU), New Delhi for providing the facilities of characterizations. We thank Dr. Saima Aijaz of Special Centre for Molecular Medicine (SCMM), JNU for providing the MDCK-2 Cell lines. This work was supported by a grant received from DST, Government of India and UGC funded UPE-II project No. 58.

References

1. Fu, F.; Wang, Q.; *J. Environ. Manage.*, **2011**, *92*, 407.
2. Wang, Y. H.; Lin, S. H.; Juang, R. S; *J. Hazard. Mater.*, **2003**, *102*, 291.
3. Järup, L.; *British Medical Bulletin*, **2003**, *68*, 167.
4. Pronczuk, J.; Brune, M.; Gore, F. (Eds.); Encyclopedia of Environmental Health, **2011**, 601.
5. Guidelines for drinking-water quality, Geneva; *World Health Organization (WHO)*, **2008**.
6. Indian standard drinking water specifications, (2nd Eds.), New Delhi, India; *Bureau of Indian Standards (BIS)*, **2012**.
7. Drinking water standard and health advisories table, San Francisco; *United States Environmental Protection Agency (USEPA)*, **2007**.
8. Martins, B. L.; Cruz, C. C.; Luna, A. S.; Henriques, C. A; *Biochemical Engineering Journal*, **2006,** *27*, 310.
9. Batley, G.; Farrar, Y.; *Anal. Chim. Acta*, **1978**, 99, 283.
10. Rykowska, I.; Wasiak, W.; Byra; *J. Chemical Papers*, **2008**, *62*, 255.
11. Zamboulis, D.; Peleka, E. N.; Lazaridis, N. K.; Matis, K. A.; *J. Chem. Technol. Biotechnol.*, **2011**, *86*, 335.
12. Li, K.; Wang, X.; *Bioresource Technology*, **2009**, *100*, 2810.
13. Oubagaranadin, J. U. K.; Murthy, Z.; *Ind. Eng. Chem. Res.*, **2009**, *48*, 10627.
14. Sun, S.; Wang, L.; Wang, A.; *J. Hazard. Mater.*, **2006a**, *136*, 930.
15. Wang, X.; Zheng, Y.; Wang, A.; *J. Hazard. Mater.*, **2009**, *168*, 970.
16. Li, X. Q.; Elliott, D.; W, Zhang.; W.X.; *Critical Reviews in Solid State and Materials Sciences*, **2006**, *31*, 111.
17. Liu, Q.; Bei, Y.; Zhou, F.; *Cent. Eur. J. Chem.*, **2009a**. *7*, 79.
18. Lee, K. J.; Lee, Y.; Yoon, J.; Kamala-Kannan, S.; Park, S. M.; Oh, B. T.; *Environmental Technology*, **2009**, *30*, 1425.
19. Cao, J.; Elliott, D.; Zhang, W. X.; *J. Nanopart. Res.*, **2005**, *7*, 499.
20. Liu, T.; Rao, P.; Lo, I. M.; *Sci. Total. Environ.*, **2009b**, *407*, 3407.
21. Ponder, S. M.; Darab, J. G.; Mallouk, T. E.; *Environ. Sci. Technol.*, **2000**, *34*, 2564.
22. Quinn, J.; Geiger, C.; Clausen, C.; Brooks, K.; Coon, C.; O'Hara, S.; Krug, T.; Major, D.; Yoon, W. S.; Gavaskar, A.; *Environ. Sci. Technol.*, **2005**, *39*, 1309.
23. Wang, W.; Zhou, M.; Mao, Q.; Yue, J.; Wang, X.; *Catal. Commun.*, **2010**, *11*, 937.
24. Yoon, I. H.; Kim, K. W.; Bang, S; Choe, E.; Lippincott, L.; *Appl. Catal. B-Environ.*, **2011**, *104*, 185.
25. Arshadi, M.; Soleymanzadeh, M.; Salvacion, J., Salimi Vahid, F.; *J. Colloid Interface Sci.*, **2014,** *426*, 241.
26. Esfahani, A. R.; Firouzi, A. F.; Sayyad, G.; Kiasat, A.; *Research Journal of Environmental and Earth Sciences*, **2013**, *5*, 548.
27. Kim, S. A.; Kamala-Kannan, S.; Lee, K. J.; Park, Y. J.; Shea, P. J.; Lee, W. H.; Kim, H.M.; Oh, B.T.; *Chemical Engineering Journal*, **2013**, *217*, 54.
28. Zhang, X.; Lin, S.; Chen, Z.; Megharaj, M.; Naidu, R.; *Water Research*, **2011,** *45*, 3481.
29. Crane, R.; Scott, T.; *Journal of Nanotechnology*, **2013**, *11*, 173625,
30. Langmuir, I.; *J. Am. Chem. Soc.*, **1918**, *40*, 1361.
31. Ho, Y. S.; McKay, G.; *Process Biochemistry*, **1999**, *34*, 451.
32. Gilbert, B.; Frandsen, C.; Maxey, E.; Sherman, D.; *Phys. Rev.*, **2009**, *79*, 035108.
33. Park, J.; Kim, S.; Choi, S.; Lee, H.; *New Physics*, **2013**, *63*, 818.
34. Wen, S. X.; Wang, Y. D.; Wang, Z. L.; Yang, S.; *J. Phys. Chem. B.*, **2005**, *109*, 215.
35. Elliott, D. W.; Zhang, W. X.; *Environ. Sci. Technol.*, **2001**, *35*, 4922.
36. Rajput, S.; Pittman, C. U.; Mohan, D.; *J. Colloid Interface Sci.*, **2015**, *468*, 334.
37. Kumari, M.; Pittman, C. U.; Mohan, D.; *J. Colloid Interface Sci.*, **2015**, *442*, 120.
38. Xin, X.; Wei, Q.; Yang, J.; Yan, L.; Feng, R.; Chen, G.; Du, B.; Li, H.; *Chemical Engineering Journal*, **2012**, *184*, 132.
39. Madrakian, T.; Afkhami, A.; Ahmadi, M.; *Chemosphere*, **2013**, *90*, 542.
40. Jabeen, H.; Christian Kemp, K.; Chandra, V.; *Journal of Environmental Management*, **2013**, *130*, 429.
41. Mahdavi, M.; Ahmad, M. B.; Jelas Haron, M. D.; Gharayebi, Y.; Shameli, K.; Nadi, B.; *J. Inorg. Organomet. Polym.*, **2013**, *23*, 599.

